J. Membrane Biol. 159, 197–208 (1997)

The Journal of
Membrane
Biology

Kinetics of Chloride-Bicarbonate Exchange Across the Human Red Blood Cell Membrane

F.A. Greco, A.K. Solomon
The Biophysical Laboratory, Harvard Medical School, Boston, MA 02115, USA

Received: 13 March 1997/Revised: 19 May 1997

Abstract. We use a fluorescent probe of $[Cl^-]$, 6-methoxy-N-(3-sulfopropyl)quinolinium (SPQ), to study Cl^-/HCO_3^- exchange in human erythrocyte ghosts in a stopped-flow apparatus at 4°C. The quench constant of SPQ in our $Cl^-/HCO_3^-/HPO_4^=$ system at pH 7.4 is 0.065 ± 0.005 mM^{-1}. The time course of Cl^-/HCO_3^- exchange does not follow a single exponential function at 4°C and we propose an extended ping-pong model in which slippage is explicitly considered in order to account for this phenomenon. The solution of the system of equations generated by our model is a double exponential function which fits the time course of Cl^-/HCO_3^- exchange. Our results confirm the predictions of the model concerning the functional dependence of the two rate constants. One rate constant (k_1) is independent of medium composition; it is determined by the sum of the two slippage rate constants and its value is 1.04 ± 0.14 sec^{-1}. The other rate constant (k_2) varies inversely with $[Cl^-]$; the regression line is $1/k_2 = 18.8\ sec - 0.095\ mM^{-1}sec\ [Cl^-]$.

Key words: Band 3 — Anion exchange — Erythrocytes — Ping-pong model — SPQ — DIDS

Introduction

Cl^-/HCO_3^- exchangers play a central role in the regulation of intracellular pH, volume, and $[Cl^-]$ and in the transport of ions across epithelial surfaces (Alper, 1991; Tanner, 1993). Of these, the erythrocyte anion exchanger (band 3, AE1) has been the most extensively studied (Knauf, 1979; Passow, 1986; Jennings, 1992). In the erythrocyte the primary function of anion exchange is the excretion of CO_2 through the chloride, or Hamburger, shift. Although several explanations have been proposed for this one-for-one exchange, the bulk of the evidence favors a model which derives from a reaction sequence in enzyme kinetics which Cleland (1963) has called the ping-pong mechanism. As applied to band 3 (Fröhlich & Gunn, 1986; Gasbjerg, Knauf & Brahm, 1996; Knauf, Gasbjerg & Brahm, 1996), the ping-pong model posits the existence of a transfer site which can bind either Cl^- or HCO_3^-; the transfer site acts as a carrier to transport anions across the membrane by a conformational change in band 3. The movement of an unloaded transfer site across the membrane, slippage, occurs more slowly by four orders of magnitude than that of loaded sites, and terms describing slippage are dropped from the kinetic equations in the standard development of the ping-pong model (Passow, 1986; Jennings, 1992). However, several phenomena have been explained by slippage, and, indeed, have provided crucial evidence in distinguishing among the various models of red cell anion exchange (Jennings, 1982; Knauf, Law & Marchant, 1983; Fröhlich, 1984). Even though the justification for neglecting slippage is empirical (Passow, 1986), most workers in the field invoke it as a postulate and obtain one-for-one exchange as a direct consequence (Passow, 1986; Jennings, 1992).

A variety of experimental techniques have been employed in the study of anion exchange. Several laboratories have used variants of the Jacobs-Stewart cycle by measuring pH or $[Cl^-]$ (Chow, Crandall & Forster, 1976; Klocke, 1976; Lambert & Lowe, 1980). Falke and Chan (1985) have measured $^{35}Cl^-$ NMR line broadening and have demonstrated that their data support the ping-pong model for anion exchange. Beginning with Tosteson's (1959) experiments, an extensive literature has emerged on the use of isotope techniques in the study of anion exchange (Gasbjerg & Brahm, 1991; Gasbjerg et al., 1996; Knauf et al., 1996). Recently Calafut and Dix (1995) have employed a fluorescent probe of $[Cl^-]$, 6-methoxy-N-(3-sulfopropyl)quinolinium (SPQ), to

Correspondence to: A.K. Solomon

monitor anion exchange in erythrocyte ghosts at room temperature.

When we undertook a series of stopped-flow experiments using SPQ in erythrocyte ghosts at 4°C, it became apparent that the time course of anion exchange could not be fit by a single exponential function, a finding not consistent with the standard view of the ping-pong model. This paper solves the ping-pong model without dropping the terms describing slippage. The resulting equation is a double exponential function. The only aspect of the solution dependent upon our experimental design is the assumption that the external [Cl^-] and [HCO_3^-] remain constant; the material presented in the Theory section below is, therefore, substantially independent of the experimental results which confirm its predictions. Within the framework of this model, the time course of anion exchange does not follow a single exponential at 4°C because of a transient during which the unloaded transfer sites adjust to the new environment after mixing. We will follow the traditional terminology and refer to the transfer site as a carrier; however, the model makes no assumptions about the physical nature of the transport step and includes non-carrier theories as well (Baker & Baker, 1996).

Theory

Figure 1 shows the ping-pong model for anion exchange with slippage and defines the symbols used below. The validity of the assumptions made both in defining the model and in simplifying the equations will be treated in the discussion. Although the variables are all functions of time, this will not be explicitly written unless it is necessary to distinguish the variable from its value at a particular instant, e.g., $C^i(t)$ from $C^i(0)$. The model generates the following system of equations:

$$\frac{dP_U^i}{dt} = c_{-1}P_C^i - c_1P_U^iC^i + b_{-1}P_B^i - b_1P_U^iB^i - u_{12}P_U^i + u_{21}P_U^o \quad (1)$$

$$\frac{dP_B^i}{dt} = -(b_{-1} + b_{12})P_B^i + b_1P_U^iB^i + b_{21}P_B^o \quad (2)$$

$$\frac{dP_C^i}{dt} = -(c_{-1} + c_{12})P_C^i + c_1P_U^iC^i + c_{21}P_C^o \quad (3)$$

$$\frac{dP_U^o}{dt} = c_{-2}P_C^o - c_2P_U^oC^o + b_{-2}P_B^o - b_2P_U^oB^o + u_{12}P_U^i - u_{21}P_U^o \quad (4)$$

$$\frac{dP_B^o}{dt} = -(b_{-2} + b_{21})P_B^o + b_2P_U^oB^o + b_{12}P_B^i \quad (5)$$

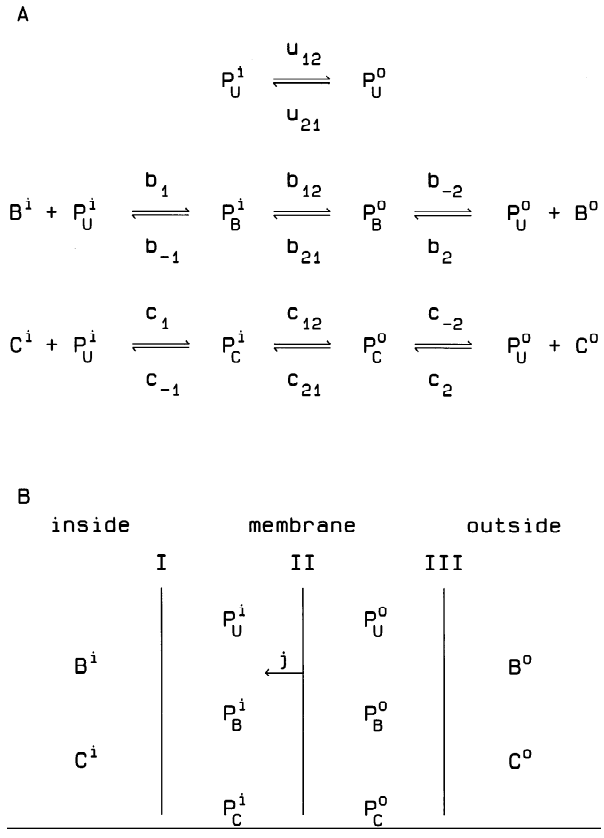

Fig. 1. Ping-pong model of anion exchange. Figure 1*A* illustrates schematically the reaction mechanism. Superscripts *i* and *o* indicate inside and outside of the cell. Capital letters *B*, *C* and *P* refer to bicarbonate, chloride and protein (band 3) concentrations. Subscripts to *P* indicate whether the transfer site is unoccupied (*U*) or binds bicarbonate (*B*) or chloride (*C*). Lower case letters *u*, *b* and *c* are the apparent rate constants. Figure 1*B* shows the physical picture corresponding to the reaction scheme above. There are three surfaces of discontinuity (I, II and III). Two of them (I and III) coincide with the physical interfaces between aqueous phase and membrane; the other (II) is theoretical, dividing the inner and outer halves of the membrane. Each anion has a net flux (*j*) through each surface and the arrow (drawn only for surface II) indicates that the reference (positive) direction for fluxes is inward. The flow of unloaded carrier, j_U^{II}, occurs only across surface II.

$$\frac{dP_C^o}{dt} = -(c_{-2} + c_{21})P_C^o + c_2P_U^oC^o + c_{12}P_C^i \quad (6)$$

$$j_C^I = c_{-1}P_C^i - c_1P_U^iC^i \quad (7)$$

$$j_B^I = b_{-1}P_B^i - b_1P_U^iB^i \quad (8)$$

$$j_C^{III} = -c_{-2}P_C^o + c_2P_U^oC^o \quad (9)$$

$$j_B^{III} = -b_{-2}P_B^o + b_2P_U^oB^o \quad (10)$$

We introduce the following fluxes through surface II:

$$j_C^{II} = c_{21}P_C^o - c_{12}P_C^i \tag{11}$$

$$j_B^{II} = b_{21}P_B^o - b_{12}P_B^i \tag{12}$$

$$j_U^{II} = u_{21}P_U^o - u_{12}P_U^i \tag{13}$$

The fluxes defined in Eq. 7–13 allow us to recast equations 1–6 in a more intuitive and compact form. Equation 3 may be rewritten as

$$\frac{dP_C^i}{dt} = j_C^{II} - j_C^I \tag{3a}$$

We make the usual assumption that the association-dissociation steps are not rate-limiting for transport (Knauf, 1979; Passow, 1986; Falke, Kanes & Chan, 1985). More precisely, we assume the following:

$$c_{-1}P_T^i >> |j_C^I| \tag{14}$$

$$b_{-1}P_T^i >> |j_B^I| \tag{15}$$

$$c_{-2}P_T^o >> |j_C^{III}| \tag{16}$$

$$b_{-2}P_T^o >> |j_B^{III}| \tag{17}$$

in which P_T^i and P_T^o stand for the total concentration of transfer sites on the inside and outside faces respectively. Using A for cell surface area and V^i for cell volume, we further assume

$$\frac{c_1P_U^i}{c_{-1}}\frac{A}{V^i} << 1 \tag{18}$$

$$\frac{b_1P_U^i}{b_{-1}}\frac{A}{V^i} << 1 \tag{19}$$

We impose the physical constraint that the two aqueous phases remain electroneutral, from which it follows that

$$j_C^I + j_B^I = 0 \tag{20}$$

$$j_C^{III} + j_B^{III} = 0 \tag{21}$$

To solve this system of equations we must introduce one approximation unique to our experimental design. The hematocrit after mixing is about 1% which allows us to use the approximation that the concentrations in the external aqueous phase remain constant, i.e.,

$$C^o = \text{constant} \tag{22}$$

$$B^o = \text{constant} \tag{23}$$

Hence B^o and C^o are also the equilibrium values.

Assumptions 14–23 above are sufficient to reduce the system of equations to a solvable differential equation. We first divide equations 7–10 by the appropriate product of dissociation constant and P_T^i or P_T^o. Using assumptions 14–17 to set to zero the left hand side of each equation and rearranging, we can write

$$P_C^i = \frac{C^i}{K_C^i}P_U^i \qquad \text{where} \quad K_C^i = \frac{c_{-1}}{c_1} \tag{24}$$

$$P_B^i = \frac{B^i}{K_B^i}P_U^i \qquad \text{where} \quad K_B^i = \frac{b_{-1}}{b_1} \tag{25}$$

$$P_C^o = \frac{C^o}{K_C^o}P_U^o \qquad \text{where} \quad K_C^o = \frac{c_{-2}}{c_1} \tag{26}$$

$$P_B^o = \frac{B^o}{K_B^o}P_U^o \qquad \text{where} \quad K_B^o = \frac{b_{-2}}{b_2} \tag{27}$$

To solve for $C^i(t)$, we rearrange Eq. 3a and multiply by the cell surface to volume ratio to convert j_C^I to dC^i/dt.

$$\frac{dC^i}{dt} = \frac{A}{V^i}j_C^I = \frac{A}{V^i}\left(j_C^{II} - \frac{dP_C^i}{dt}\right) \tag{28}$$

We can use equations 24 and 26 to rewrite Eq. 11 for j_C^{II}. Substituting the result into Eq. 28 and rearranging gives

$$\frac{dC^i}{dt} = \frac{A}{V^i}\frac{c_{21}}{K_C^o}C^oP_U^o - \frac{A}{V^i}\frac{c_{12}}{K_C^i}C^iP_U^i - \frac{A}{V^i}\frac{dP_C^i}{dt} \tag{29}$$

Equation 29 corresponds to Passow's (1986) Eq. 9, Knauf's (1979) Eq. 13, and Fröhlich and Gunn's (1986) Eq. 4. Substituting Eq. 24 into 29 for P_C^i, differentiating and rearranging gives

$$\left(1 + \frac{A}{V^i}\frac{P_U^i}{K_C^i}\right)\frac{dC^i}{dt} = \frac{A}{V^i}\frac{c_{21}}{K_C^o}P_U^oC^o - \left(\frac{A}{V^i}\frac{c_{12}}{K_C^i}P_U^i + \frac{A}{V^i}\frac{1}{K_C^i}\frac{dP_U^i}{dt}\right)C^i \tag{30}$$

By assumption 18 the coefficient of dC^i/dt may be taken as 1, giving

$$\frac{dC^i}{dt} = \frac{A}{V^i}\frac{c_{21}}{K_C^o}P_U^oC^o - \left(\frac{A}{V^i}\frac{c_{12}}{K_C^i}P_U^i + \frac{A}{V^i}\frac{1}{K_C^i}\frac{dP_U^i}{dt}\right)C^i \tag{31}$$

An expression for dB^i/dt may be derived by, *mutatis mutandis*, repeating the argument above beginning at Eq. 2. The resulting expression is

$$\frac{dB^i}{dt} = \frac{A}{V^i}\frac{b_{21}}{K_B^o}P_U^o B^o - \left(\frac{A}{V^i}\frac{b_{12}}{K_B^i}P_U^i + \frac{A}{V^i}\frac{1}{K_B^i}\frac{dP_U^i}{dt}\right)B^i \quad (32)$$

EQUATIONS FOR v_0

Even without solving Eq. 31 and 32, we may use them to derive relations for the initial velocity, v_0. For experiments in which $C^i(0) = 0$, it is simplest to take v_0 as dC^i/dt at $t = 0$. In this case equation 31 becomes

$$v_0 = \frac{A}{V^i}\frac{c_{21}}{K_C^o}P_U^o(0)C^o \qquad [C^i(0) = 0] \quad (33)$$

We may derive an expression for $P_U^o(0)$ as follows. Let $P_T^o(t < 0)$ be the total concentration of transfer sites per unit area on the outside of the membrane prior to mixing. At $t = 0$, immediately after mixing, the dissociation reactions equilibrate before there can be any significant change in the number of transfer sites (assumptions 16 and 17). Therefore,

$$P_T^o(t<0) = P_U^o(0) + P_U^o(0)\frac{C^o}{K_C^o} + P_U^o(0)\frac{B^o}{K_B^o}$$

which can be rearranged to

$$P_U^o(0) = \frac{P_T^o(t<0)}{1 + \dfrac{C^o}{K_C^o} + \dfrac{B^o}{K_B^o}} \quad (34)$$

In our experiments, $B^o + C^o = 0.15$ M. Using this to eliminate B^o and substituting Eq. 34 into 33 leads to

$$v_0 = \frac{\left(\dfrac{A}{V^i}\dfrac{c_{21}}{K_C^o}P_T^o(t<0)\right)C^o}{\left(1 + \dfrac{0.15}{K_B^o}\right) + \left(\dfrac{1}{K_C^o} - \dfrac{1}{K_B^o}\right)C^o} \qquad [C^i(0) = 0] \quad (35)$$

Equation 35 entails that a plot of $1/v_0$ against $1/C^o$ should be a straight line for the experiments in which $C^i(0) = 0$. For the experiments in which $B^i(0) = 0$, Eq. 32 becomes

$$\frac{dB^i}{dt} = \frac{A}{V^i}\frac{b_{21}}{K_B^o}P_U^o B^o \qquad [B^i(0) = 0] \quad (36)$$

For these measurements we take v_0 as dB^i/dt at $t = 0$ and note that equation 20 entails that $dB^i/dt = -dC^i/dt$. Proceeding as before, *mutatis mutandis*, leads to

$$v_0 = \frac{\left(\dfrac{A}{V^i}\dfrac{b_{21}}{K_B^o}P_T^o(t<0)\right)B^o}{\left(1 + \dfrac{0.15}{K_C^o}\right) + \left(\dfrac{1}{K_B^o} - \dfrac{1}{K_C^o}\right)B^o} \qquad [B^i(0) = 0] \quad (37)$$

Equation 37 necessitates that a plot of $1/v_0$ against $1/B^o$ fall on a straight line for experiments in which $B^i(0) = 0$.

EQUATION FOR $C^i(t)$

We may integrate Eq. 31 by making the further assumption that the state after mixing is not too far from equilibrium. Using $\overline{P}_U^i$ to be the equilibrium value of P_U^i, P^T to be the total concentration of band 3 per unit area, and letting $u_{12}/u_{21} = K_U$, the solution is

$$C^i(t) = a_1 e^{-k_1 t} + a_2 e^{-k_2 t} + C^o \quad (38)$$

where

$$k_1 = u_{21} + u_{12} \quad (39)$$

$$k_2 = \frac{A}{V^i}\frac{c_{12}}{K_C^i}\overline{P}_U^i = \frac{\dfrac{A}{V^i}\dfrac{c_{12}}{K_C^i}P^T}{1 + K_U + C^o\left(\dfrac{K_U}{K_C^o} + \dfrac{1}{K_C^i}\right) + B^o\left(\dfrac{K_U}{K_B^o} + \dfrac{1}{K_B^i}\right)} \quad (40)$$

$$a_1 = \frac{(P_U^o(0)u_{21} - P_U^i(0)u_{12})\left(\dfrac{k_1}{c_{12}} - \dfrac{1}{K_U} - 1\right)\dfrac{A}{V^i}\dfrac{c_{12}}{K_C^i}C^o}{(k_2 - k_1)(k_1)} \quad (41)$$

$$a_2 = C^i(0) - C^o - a_1 \quad (42)$$

The details of this solution are given in the Appendix. Equations 39 and 40 lead to predictions that may be rigorously tested concerning the functional form and dependence of the rate constants. One rate constant, k_1, should be independent of C^o and B^o. Given that $B^o + C^o = 0.15$M in our system, equation 40 predicts that $1/k_2$ should be proportional to C^o.

Materials and Methods

REAGENTS

SPQ, 6-methoxy-N-(3-sulfopropyl)quinolinium, (Molecular Probes, Eugene, OR) was prepared as a 20 mM stock solution in 5 mM

Na_2HPO_4, pH 8, and stored frozen in aliquots. Na_2DIDS, 4,4′-diisothiocyano-2,2′-stilbene disulfonate, was also obtained from Molecular Probes (Eugene, OR). $NaHCO_3$ solutions were freshly prepared before each experiment in 10 mM Na_2HPO_4. Each solution was adjusted to pH 7.4 and kept in a syringe anaerobically until use; pH did not change by more than 0.3 during the course of an experiment.

Hemoglobin-free Red Cell Ghosts

''White'' ghosts were resealed to contain 10 mM SPQ, 10 mM Na_2HPO_4, pH 7.4, and either 150 mM NaCl or $NaHCO_3$ in the following manner. Ghosts were prepared by a modification of the method of Steck and Kant (1974). Citrate-anticoagulated human blood was used within 24 hr of collection. Following three washes in normal saline, the cells were hemolysed in 5 mM Na_2HPO_4, pH 8, on ice. Ghosts were washed in lysing medium three times by centrifugation at 10,000 × *g* for 10 min at 4°C. 1 ml of pellet was added to 1 ml of 20 mM SPQ stock solution and incubated on ice for 5 min. Salt was added to bring the concentration to 150 mM NaCl or $NaHCO_3$. Following a second 5-min incubation on ice, the ghosts were resealed by incubation at 37°C for 1 hr. For experiments with DIDS, ghosts were resealed in 300 μM Na_2DIDS. Resealed ghosts were washed three times and the resulting pellet was resuspended 1:50 (vol/vol) in 10 mM Na_2HPO_4, pH 7.4, and either 150 mM NaCl or $NaHCO_3$.

Stopped-Flow Studies

Fluorescence measurements were performed on a Model SF.17MV Stopped-flow Spectrometer (Applied Photophysics, Leatherhead, UK). SPQ excitation was at 350 nm (9 nm bandpass) with emission measured through a 3 mm Corion cut-on filter with 50% transmission at 500 nm. Compressed air at 40 psi injected equal volumes of ghosts and Cl^-/HCO_3^- mixtures into a mixing chamber; a stop syringe (0.1 ml) triggered recording. Measurements are labeled according to $[Cl^-]$ after mixing; $[HCO_3^-] = 0.15\ \text{M} - [Cl^-]$ for all measurements. Osmolality of the 150 mM NaCl buffer was 295 ± 5 mOsm and that of the 150 mM $NaHCO_3$ buffer was 276 ± 5 mOsm as determined by freezing point depression (Fiske Model OS, Uxbridge, MA). Osmotic gradients across the red cell membrane were always less than 10 mOsm. A circulating waterbath (Model 1145, VWR, Westchester, PA) maintained the drive syringes and mixing chamber at 4 ± 0.1 °C. For most experiments four hundred data points were collected over 10 sec and stored in the spectrometer's workstation. Seven to ten replicate measurements were made at each $[Cl^-]$. Data shown are from 10 experiments done on blood from 6 individuals. A small decrease in fluorescence occurs when ghosts are mixed with their suspending buffer. This baseline was subtracted from each measurement prior to converting fluorescence to $[Cl^-]$. A mixing artifact, usually less than 25 msec, was truncated from the data before conversion.

Conversion of Fluorescence to Internal $[Cl^-]$

For solutions of NaCl the fluorescence of SPQ follows the Stern-Volmer equation

$$\frac{F_0}{F} = 1 + K[Cl^-] \tag{43}$$

where F_0 is the fluorescence at $[Cl^-] = 0$ and K is the quench constant (Illsley & Verkman, 1987; Garcia, 1992; Calafut & Dix, 1995). We confirmed that the Stern-Volmer equation also applies to our $Cl^-/HCO_3^-/HPO_4^=$ system (Fig. 2). For ghosts loaded with 150 mM $NaHCO_3$ we used the Stern-Volmer equation to convert fluorescence to internal $[Cl^-]$. The time-dependent fluorescence tracks $[Cl^-]$ inside the ghosts and we estimated the parameters F_0 and K for the internal phase as follows. Letting F_i and F_f be the initial and final measured fluorescence after mixing

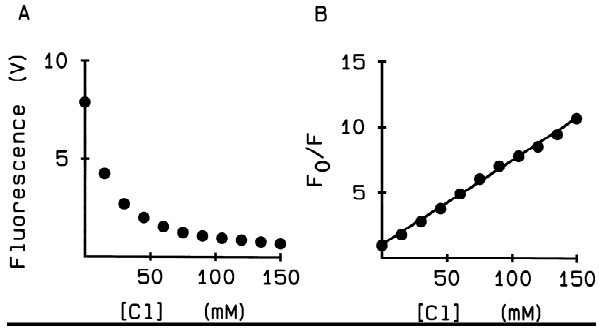

Fig. 2. Fluorescence of SPQ in aqueous solution. Panel *A* shows the fluorescence of a solution of SPQ as a function of $[Cl^-]$. Medium composition is as follows: SPQ 10 mM; Na_2HPO_4 10 mM, pH 7.4; NaCl as indicated by $[Cl^-]$; $NaHCO_3$ 150 mM − [NaCl]. Panel *B* shows the Stern-Volmer plot of the data in Panel *A*, where F_0 is the fluorescence at $[Cl^-] = 0$. The least-squares fit is 1.02 + 0.065 mM^{-1} $[Cl^-]$.

$$F_f - F_i = \Delta F_{\text{ghosts}} = \frac{F_0}{1 + K[Cl_f^-]} - \frac{F_0}{1 + K[Cl_i^-]} \tag{44}$$

which, since $[Cl_i^-] = 0$ inside the ghosts, may be rearranged to

$$\frac{1}{F_i - F_f} = \frac{1}{KF_0[Cl_f^-]} + \frac{1}{F_0} \tag{45}$$

Therefore, for ghosts loaded with 150 mM $NaHCO_3$ we obtained estimates of the Stern-Volmer parameters from a least-squares fit of $1/(F_i - F_f)$ against $1/[Cl_f^-]$ for each preparation (Fig. 3*A* and *B*). For ghosts loaded with 150 mM NaCl, a plot of $F_f - F_i$ against $[Cl_f^-] - [Cl_i^-]$ closely fit a straight line (Fig. 3*C* and *D*). Therefore, a linear conversion factor was obtained from the slope of the least-squares fit.

Curve-fitting

After converting fluorescence to internal $[Cl^-]$, eq. 38 was fit to the time course by least squares using a software package supplied with the spectrometer. Initial estimates of the parameters in Eq. 38 were obtained by fitting single exponentials to two domains: less than and greater than one second.

Results

SPQ as a Probe of $[Cl^-]$

Vasseur, Fragne and Alvarado (1993) have demonstrated the need to determine the behavior of SPQ in each system of electrolytes. Figure 2*A* shows the fluorescence of SPQ in an aqueous Cl^-/HCO_3^- system with Na_2HPO_4 buffer, pH 7.4. The fluorescence follows the Stern-

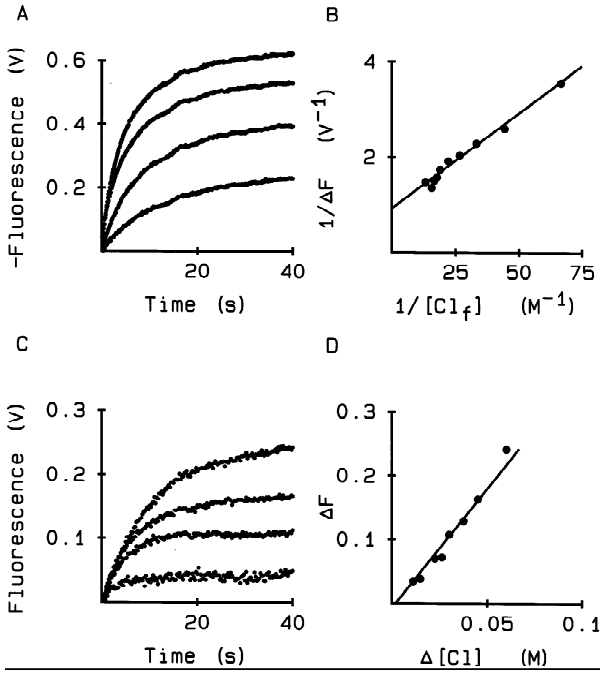

Fig. 3. Conversion of fluorescence to $[Cl^-]$. Panel *A* shows the time course of fluorescence after mixing ghosts loaded with 150 mM $NaHCO_3$ with a graded series of Cl^-/HCO_3^- mixtures. The curves have been translated to align the origins and inverted to facilitate comparison with Fig. 3*C* below. The tracings correspond in order of increasing amplitude to initial gradients of 15, 30, 45 and 60 mM, in this instance inward for Cl^-, outward for HCO_3^-. Panel *B* is a plot of $1/(F_i - F_f)$ against $1/[Cl^-_f]$, where F_i and F_f are the initial and final measured fluorescences, and illustrates the method of obtaining the Stern-Volmer parameters (Eq. 45). Panel *C* shows the time course of fluorescence after mixing ghosts loaded with 150 mM NaCl with a graded series of Cl^-/HCO_3^- mixtures. Again the curves have been translated to align the origins. The tracings correspond in order of increasing amplitude to initial gradients of 15, 30, 45, 60 mM, in this case outward for Cl^- and inward for HCO_3^-. Panel *D* is a plot of ΔF against $\Delta[Cl]$; for each point in the time course, 0.15 − $[Cl^-]$ was calculated by divinding $F(t) - F(0)$ by the slope of this plot.

Volmer equation and the regression line is 1.02 + 0.065 mM^{-1} $[Cl^-]$ (Fig. 2*B*).

In SPQ-loaded ghosts two technical difficulties arise in the use of the Stern-Volmer equation to convert fluorescence to $[Cl^-]$. First, it is not possible to measure F_0 directly. Second, because the stopped-flow syringes mix equal volumes of solutions in our system, measurements with a given preparation of ghosts could be made with $[Cl^-]$ above or below 75 mM but could not span the entire range from 0–150 mM. In aqueous solution the dependence of fluorescence upon $[Cl^-]$ becomes nearly linear above 75 mM (Fig. 2*A*) and the Stern-Volmer equation is no longer useful. Therefore, we used two methods for converting fluorescence to $[Cl^-]$ according as $[Cl^-]$ was above or below 75 mM (Fig. 3). For $[Cl^-]$ below 75 mM (Fig. 3*A* and *B*), both parameters in the Stern-Volmer equation were allowed to vary in fitting the data. The apparent quench constants obtained from these fits (0.018 ± 0.007 mM^{-1}) were always less than the quench constant in aqueous solution. For $[Cl^-]$ above 75 mM (Fig. 3*C* and *D*), fluorescence becomes linearly dependent upon $[Cl^-]$ at equilibrium.

Time Course of $[Cl^-]$ and Effect of DIDS

Acquiring data at 25 msec/point gave adequate time resolution (Fig. 4*A*) over an interval sufficient for curve-fitting (Fig. 4*B*). The time course of internal $[Cl^-]$ does not follow a single exponential function (Fig. 4*B*, upper panel); most of the deviation from a single exponential occurs within 3 sec after mixing (Fig. 4*B*). 300 μM Na_2DIDS completely abolishes anion exchange, including the transient occurring over the first 3 sec (Fig. 4*A*).

Our model predicts that the time-course of internal

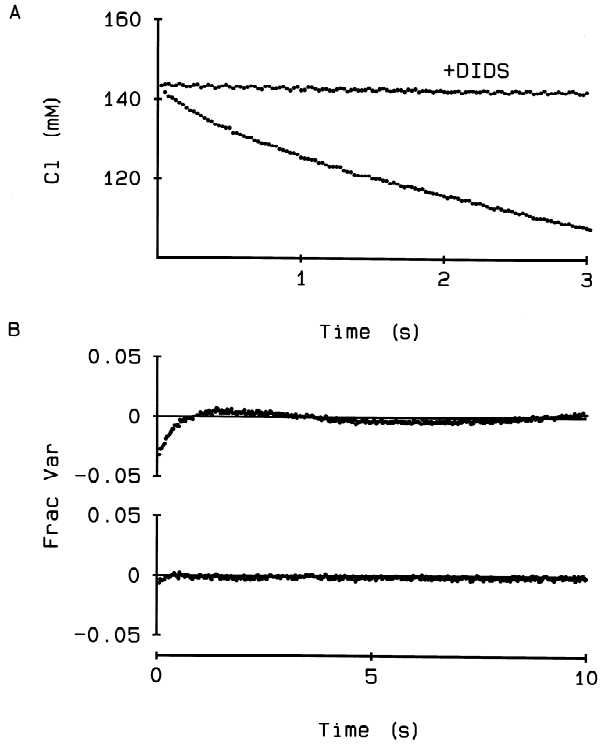

Fig. 4. Time course of internal $[Cl^-]$ and effect of DIDS. Figure 4*A* shows the initial time course of internal $[Cl^-]$ in ghosts loaded with 0.15 M NaCl in response to a 0.075 M gradient. Incubation at 37°C in 300 μM Na_2DIDS for 1 hr during the resealing step completely abolished anion exchange. In panel *B* the upper figure shows the fractional variance from a single exponential fit to the time course of $[Cl^-]$ in ghosts loaded with 0.15 M NaCl in response to a 0.075 M gradient. Note that the greatest deviation from a single exponential fit occurs over the first 3 sec. The lower figure in panel *B* is the fractional variance from a double exponential fit to the same data and illustrates the improvement by using Eq. 38. The initial estimates for this least-squares fit were obtained by fitting single exponentials to the first and last nine seconds of the time course.

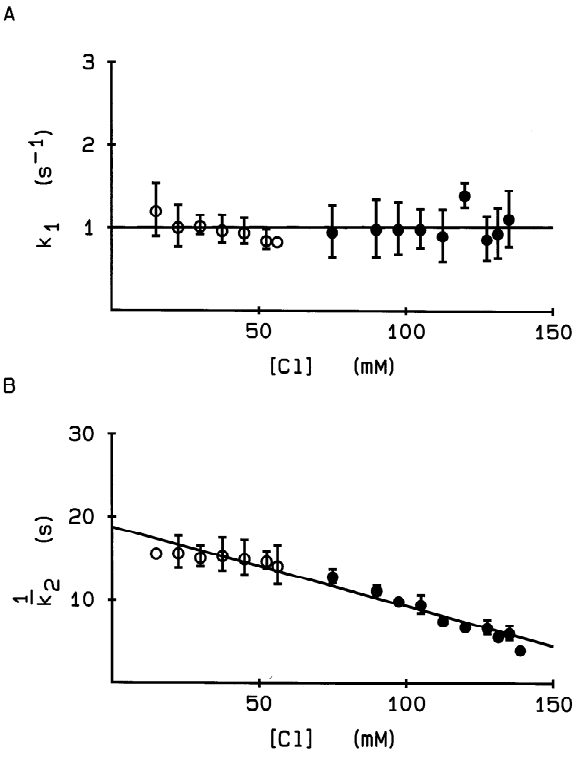

Fig. 5. Dependence of rate constants upon medium composition. Rate constants k_1 and k_2 were obtained by fitting Eq. 38 to the time course of [Cl^-]. Concentrations are equilibrium concentrations after mixing, C^o in the Theory section. [HCO_3^-], ie., B^o, is given by 150 mM − [Cl^-]. Open circles are data obtained from ghosts loaded with 150 mM $NaHCO_3$ and represent inward Cl^- gradients and outward HCO_3^- gradients. Filled circles are data obtained from ghosts loaded with 150 mM NaCl and represent outward Cl^- and inward HCO_3^- gradients. Panel *A* shows k_1 against [Cl^-]. As predicted by Eq. 39, k_1 does not depend upon medium composition; its value from the regression line is 1.04 ± 0.14 sec^{-1}. Panel *B* is plot of $1/k_2$ against [Cl^-]. As predicted by the model (Eq. 40), this plot is a straight line; the regression line is $1/k_2$ = 18.8 sec − 0.095 mM^{-1}sec [Cl^-]. Error bars that fall inside a symbol have been omitted.

[Cl^-] should follow a double exponential function (Eq. 38). Figure 4*B* shows that using a double exponential function (lower panel) improves the fit in comparison to a single exponential (upper panel). The rate constants from fitting Eq. 38 are shown in Fig. 5. Rate constant k_1 is independent of medium composition for both inward and outward Cl^- gradients (Fig. 5*A*); its average value is 1.04 ± 0.14 sec^{-1}. Rate constant k_2 varies inversely with [Cl^-], consistent with eq. 40 after substituting $B^o = 0.15 - C^o$ (Fig. 5*B*). This relation holds for both inward and outward Cl^- gradients; the regression line is $1/k_2$ = 18.8 sec − 0.095 mM^{-1}sec [Cl^-].

Initial Velocity as a Function of Medium Composition

Equation 35 predicts that the double reciprocal plot of $1/v_0$ against $1/C^o$ should fall on a straight line for ghosts loaded with 0.15M $NaHCO_3$; Figure 6*A* shows that the data confirm this prediction. The least squares fit to this line is $1/v_0 = 10\ (1/C^o) - 52$. Similarly, Eq. 37 predicts that plotting $1/v_0$ against $1/B^o$ should yield a straight line for experiments in which ghosts loaded with 0.15 M NaCl (Fig. 6*B*). The least squares fit to this line is $1/v_0 = 3.2\ (1/B^o) + 63$.

Discussion

Calafut and Dix (1995) have used SPQ to study Cl^-/HCO_3^- exchange in erythrocyte ghosts at room temperature. Their value of the quench constant in aqueous Cl^-/HCO_3^- solutions with HEPES buffer was 0.071 ± 0.017 mM^{-1}, which agrees within experimental error with our value of 0.065 ± 0.005 mM^{-1} in phosphate buffer. The quench constant in NaCl or KCl solution is 0.117 ± 0.001 mM^{-1} (Illsley & Verkman, 1988; Zhang & Solomon, 1992; Calafut & Dix, 1995). These findings underscore the importance of determining the quench constant for

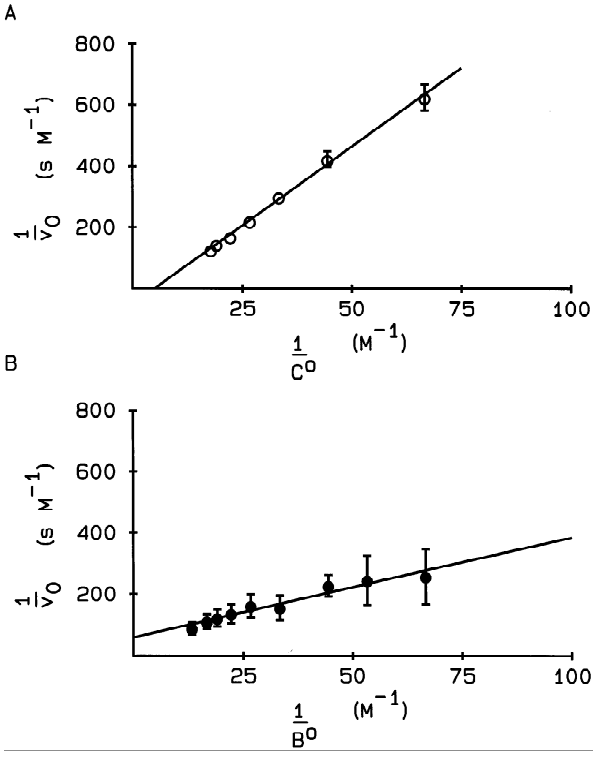

Fig. 6. Dependence of initial velocity on medium composition. Panel *A* is a double reciprocal plot, $1/v_0$ against $1/C^o$, for ghosts initially loaded with 0.15 M $NaHCO_3$. v_0 is dC^i/dt at $t = 0$. As predicted by Eq. 35 the points fall on a straight line; the equation of the regression line is $1/v_0 = 10\ (1/C^o) - 52$. Figure 6*B* is a double reciprocal plot of $1/v_0$ against $1/B^o$ for ghosts initially loaded with 0.15 M NaCl. v_0 is dB^i/dt at $t = 0$. Equation 37 predicts that these points should fall on a straight line; the equation of the regression line is $1/v_0 = 3.2\ (1/B^o) + 63$. Error bars have been omitted when they fall inside the symbol.

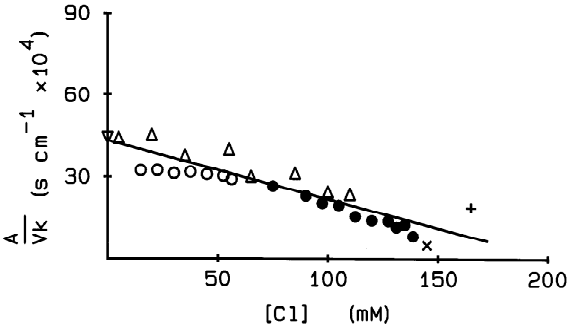

Fig. 7. Comparison with published values of anion exchange at low temperature. For a transport process described by a single exponential function with rate constant k, $k V^i/A$ is the effective permeability when the external compartment is large. The reciprocal of this value plotted against equilibrium $[Cl^-]$ should be a straight line according to our model (Eq. 40). This figure compares the values of $k V^i/A$ from the literature with those calculated from k_2 in this paper. The key to the symbols is as follows: ○ - this paper, Cl^- influx; ● - this paper, Cl^- efflux; ▽ - ^{36}Cl efflux into HCO_3^- medium, erythrocytes (Dalmark, 1972); △ - ^{36}Cl efflux, equilibrium exchange in erythrocytes (Dalmark, 1972); X - Jacobs-Stewart cycle, erythrocytes (Chow et al., 1976); + - ^{36}Cl efflux, equilibrium exchange in erythrocytes and 1-step ghosts (Funder & Wieth, 1976). All values are adjusted to 4°C, pH 7.4. Dalmark's (1972) ^{36}Cl equilibrium exchange data (his Fig. 4) were adjusted to a red cell surface area of 143 μm^2 (Funder & Wieth, 1976) and plotted according to $[Cl^-]$. The datum from Chow et al. (1976) was calculated directly from the rate constant assuming a surface-to-volume ratio of 1.6×10^4 cm^{-1} (Funder & Wieth, 1976) and was plotted according to $[HCO_3^-]$. The mean corpuscular volume of our hemoglobin-free resealed ghosts is about 0.8 of the initial value and we have taken A/V^i to be 2.1×10^4 cm^{-1}. The regression line of all data is $43 - 0.21[Cl^-]$, where $[Cl^-]$ is in mM.

each system of electrolytes (Garcia, 1992; Vasseur et al., 1993). Moreover, they raise the question of how to determine the quench constant in a biological system. The equilibrium values of the time-dependent fluorescence clearly obey the Stern-Volmer equation (Fig. 3*B*) but the apparent quench constant from a two-parameter fit is less than a third of that in aqueous solution. These considerations lead us to abandon the technique of assuming that the quench constant in the biological system is the same as that in aqueous solution and to treat the equilibrium values of the time-dependent fluorescence as determining a standard curve. Depending upon the concentration range, we used either a straight line or hyperbola to fit the standard curve. The justification for this empirical approach lies in its success. Figure 5 shows no discontinuity between the two ranges of $[Cl^-]$, which supports the consistency of the methods for converting fluorescence to $[Cl^-]$. Furthermore, Fig. 7 indicates that our values for the exchange rate agree with those obtained by other investigators at low temperature.

While our scheme for ping-pong kinetics is identical to that of other authors (Knauf, 1979; Passow, 1986; Fröhlich & Gunn, 1986), our approach to its solution differs somewhat. The standard treatment of a carrier mechanism is to assume a steady state in which the number of transfer sites on each side of the membrane remains constant (Schultz, 1980; Neame & Richards, 1972). Such an approach leads to equations relating initial velocities and concentrations that are formally similar to Michaelis-Menten kinetics. It also predicts that the time course should follow a single exponential function (Calafut & Dix, 1995). Our data never followed a single exponential function of time (Fig. 4) but rather suggested an initial transient in approach to a steady state. The success of our model in predicting the functional dependence of the rate constants (Fig. 5) makes it one possible explanation of the phenomenon and we now turn to eliminate other possibilities.

The possibility that a subpopulation of smaller ghosts may account for the early time course may be eliminated by the failure of k_1 to depend upon $[Cl^-]$ and by the observation that no such dimorphism is seen by microscopic examination. That DIDS abolished the initial transient in C^i (Fig. 4*A*) strongly suggests the involvement of an anion exchange protein (Knauf, 1979; Passow, 1986) as opposed to a process in the lipid bilayer or diffusion through an unsealed hole. The only gradients across the membrane that might theoretically be coupled to and thereby interfere with the measurement of Cl^-/HCO_3^- exchange are dissolved CO_2 and $CO_3^=$. As will appear, interference by these species is unlikely because the gradients are too small and any coupling reaction too slow. From the data of Magid and Turbeck (1968), it may be estimated that under the conditions of our measurements (T = 4°C, pH = 7.4, all CO_2 from $NaHCO_3$) approximately 98% of total CO_2 will be in the form of HCO_3^-, 1% will be in the form of dissolved CO_2 and H_2CO_3, and 1% in the form of $CO_3^=$. Even in the extreme case when ghosts loaded with 0.15 M NaCl are mixed with 0.15 M $NaHCO_3$, the inward gradients of CO_2 and $CO_3^=$ are less than 1.5 mM, too small to have a measurable effect. What CO_2 may cross the membrane will remain in that form and not be coupled with Cl^-/HCO_3^- exchange. Erythrocyte ghosts have no demonstrable carbonic anhydrase activity (London, Lipkowitz & Abramson, 1987; Calafut & Dix, 1995) and at 4°C the half-time of uncatalyzed hydration of CO_2 is 150 sec (Magid & Turbeck, 1968), which is two orders of magnitude slower than the process of interest. Although no data are available on the transport of $CO_3^=$ across red blood cell membranes, in general divalent anions are transported more slowly than monovalent anions by several orders of magnitude (Knauf, 1979). Given that the early time course reflects protein-mediated anion exchange, it may theoretically be due to a protein other than band 3, a possibility that may be dismissed rather quickly. Even though the additional process reaches equilibrium within a few seconds, it accounts for up to 10% of the total anion exchange (*data not shown*). To

postulate a second anion exchange protein with such efficacy would gainsay the large body of data on inhibitors that show that band 3 accounts for virtually all anion exchange in erythrocytes (Knauf, 1979). We conclude, therefore, that the additional process represents a transient in the state of band 3 in the membrane, which can be explained in the ping-pong model by a change in the number of transfer sites on either side of the membrane in response to the new environment.

The assumptions of our model are straightforward. Because there is virtually no protein inside white ghosts (Schwoch & Passow, 1973), there is no need to consider the Donnan equilibrium. Furthermore, our salt concentrations remain below 150 mM and we do not include a modifier site (Dalmark, 1976). Our assumptions 14–17, that the dissociation steps are not rate-limiting, have been confirmed experimentally by Falke et al. (1985). Assumption 18, i.e.,

$$\frac{P_U^i}{K_C^i}\frac{A}{V^i} << 1$$

is more novel. Given that $P_U^i < P^T$, that $P^T \approx 10^{-12}$ moles/cm^2, and that $A/V^i \approx 10^4$ cm^{-1}, we can write

$$\frac{P_U^i}{K_C^i}\frac{A}{V^i} < \frac{10^{-5}}{K_C^i} \tag{46}$$

Therefore, as long as $K_C^i > 10^{-4}$ M, approximation 18 will be valid. Current estimates of K_C^i exceed this cutoff (Jennings, 1992) and approximation 18 is well-founded.

As mentioned above, most treatments of carrier-mediated transport assume that the process is in a steady state in which the total number of transfer sites on each side of the membrane remains constant. Within the literature on band 3, it has long been recognized that the distribution of transfer sites depends upon the composition of the medium. However, studies to date have focused on the importance of recruitment to distinguish among the various models of anion exchange (Passow, 1986; Knauf et al., 1983; Jennings, 1982) and on the role of slippage in conductive Cl^- transport (Knauf et al., 1983; Fröhlich, Liebson & Gunn, 1983; Fröhlich, 1984). In the standard ping-pong model (Fröhlich & Gunn, 1986; Passow, 1986), the assumptions of a steady-state and no slippage satisfy electroneutrality and it is not imposed as an independent condition upon the model; however, these two assumptions do not allow a transient in the state of the membrane. Our assumption of electroneutrality concerns surfaces I and III (Fig. 1): $j_C^I + j_B^I = 0$ and $j_C^{III} + j_B^{III} = 0$. Electroneutrality here plays the same role as in Kohlrausch's theory of electrolyte conductance. The only connection between electroneutrality and a property of band 3 is the straightforward assumption that the dissociation step is very fast. We do not invoke electroneutrality to constrain the flows of Cl^- and HCO_3^- through surface II. Whether the flows across surface II are constrained by electroneutrality depends upon whether or not the band 3-anion complex is charged; this is not known and our model makes no assumptions regarding it. However, any difference between the flows through II and those through I and III must occur through a change in the number of ions bound to band 3. Because the flows through the red cell membrane in our experiments are on the order of 10^8 ions/sec and there are only 10^6 copies of band 3 per red cell, $j_C^{II} + j_B^{II} \approx 0$, regardless of whether or not the band 3-anion complex is neutral. Our assumptions, being less restrictive, not only allow the observed transient but also correctly predict the functional dependence of the rate constraints.

The first rate constant, k_1, is independent of medium composition and is given by $u_{12} + u_{21}$, the sum of the two slippage rates. Because conductive anion transport may occur in part by slippage (Knauf et al., 1977; Fröhlich, 1984), a simple steady-state model (assuming $dP_U^i/dt = 0 = dP_C^i/dt$) can be analyzed to show that the available data on conductive Cl^- transport are consistent with our value of 1.04 sec^{-1}. For conductive Cl^- transport, the movement of a loaded transport site is balanced in the steady state by that of an unloaded site, i.e., $j_C^{II} + j_U^{II} = 0$. Taking $C^i = 0$, we can write (from eqs. 11, 24 and 26)

$$P_U^i u_{12} = P_C^o c_{21} \tag{47}$$

Because c_{21} is several orders of magnitude larger than u_{21} or u_{12}, it follows that $P_u^i \approx P^T$. Hence

$$j_C^{II} \approx P^T u_{12} \tag{48}$$

Taking 0.5 sec^{-1} as an estimate of u_{12} and P^T as 10^{-12} moles/cm^2 give a conductive flux of 5×10^{-13} moles/cm^2 sec. Although the conductive Cl^- flux due to this model is to a first approximation independent of Cl^- gradient, an apparent permeability at 0.15 M Cl^- can be calculated by dividing the flux by the Cl^- gradient after converting the units to moles/cm^3. The resulting apparent conductive permeability at $C^o = 0.15$ M is 3.3×10^{-9} cm/sec and agrees with the value 10^{-9} cm/sec which may be obtained by extrapolation from Hunter's (1977) data. While the analysis above is at best good to an order of magnitude, it nonetheless demonstrates that our estimate of k_1 is consistent with other results that reflect slippage.

The second rate constant, k_2, corresponds to the steady-state exchange rate and therefore to the permeability of the membrane as measured by other methods. Because of the curvature in the Arrhenius plot of anion exchange (Chow et al., 1976), quantitative comparison between our data at 4°C and those obtained at tempera-

tures above 17°C is not practical. Qualitatively, our results agree with those which Calafut and Dix (1995) obtained at 25°C that the higher the equilibrium [HCO_3^-], the lower the exchange rate. However, there are sufficient data collected at low temperature to make a quantitative comparison. Dalmark (1972) used $^{36}Cl^-$ equilibrium fluxes to study the effect of varying [Cl^-] and [HCO_3^-] on exchange rate. If Dalmark's data (his Fig. 4) are replotted as our Fig. 5 (reciprocal permeability against [Cl^-]), the points also fall on a straight line as predicted by our model (Fig. 7). Although Chow et al. (1976) worked only at low [HCO_3^-], their data using a pH jump technique also agree with ours (Fig. 7). Given that these experiments employed completely independent techniques, studying both intact red cells and ghosts, the quantitative agreement of the results is quite remarkable.

At first glance our model appears to be at variance with the data of Klocke (1976); a closer examination reveals it is not. Klocke (1976) compared Cl^-/HCO_3^- exchange in ''chloride-loaded'' and ''bicarbonate-loaded'' red cells at 37°C using a continuous flow technique. He found that Cl^-/HCO_3^- exchange proceeded more slowly in the ''chloride-loaded'' cells (rate constant 5.7 sec^{-1}) than in the ''bicarbonate-loaded'' cells (rate constant 9.8 sec^{-1}), in apparent disagreement with the prediction of our model. However, our model predicts that the equilibrium values of Cl^- and HCO_3^- determine the rate constant, not the initial values. In Klocke's experiments the ''chloride-loaded'' cells after mixing were in a medium whose [HCO_3^-] was 87.5 mM; the ''bicarbonate-loaded'' cells were in a medium whose [HCO_3^-] was 73 mM. Therefore, Klocke's data also agree with the prediction that the higher the equilibrium [HCO_3^-], the slower the exchange rate.

Equations 35 and 37 for v_0 are formally similar to those of Michaelis-Menten kinetics. Indeed, if K_m and K_i are substituted for K_B^o and K_C^o, these equations become identical to that for competitive inhibition in enzyme kinetics with v_{max} equal to $(A/V^i)c_{21}P_T^o$ ($t < 0$). From this perspective, the linearity of the double reciprocal plots (Fig. 6) not only confirms the prediction of the model but also obviates the need to consider cooperative interactions among protein domains (Segel, 1975). This linearity justifies our not including a modifier site in the model (Dalmark, 1976). Unlike the usual approach to Michaelis-Menten kinetics, however, v_{max} changes during the first few seconds of the reaction; a brief examination of the reasons for the change in v_{max} will add some intuitive insight as well as show the limitations of Eqs. 35 and 37. When bicarbonate-loaded ghosts are mixed with a Cl^-/HCO_3^- solution, the outside face of the membrane equilibrates with the new medium almost as rapidly as mixing occurs, certainly in less than 1 msec. Immediately after mixing all of the loaded internal transfer sites contain HCO_3^- whereas the loaded external sites have both Cl^- and HCO_3^-. Since bicarbonate-loaded transfer sites cross the membrane (surface II) faster than chloride-loaded sites (Knauf, 1979), there will be a rapid rearrangement of the loaded sites with a net movement of bicarbonate-loaded sites from the internal to external face. This rearrangement will tend to increase the total number of transfer sites on the external face. Because all of these extra transfer sites are initially loaded, there is a disruption of the equilibrium between loaded and unloaded sites. As the loaded sites discharge their anions, the number of unloaded sites will increase but electroneutrality limits the ability of this path to restore equilibrium. Thus the flow of unloaded sites across the membrane is needed in order for the system to attain equilibrium. About the time that measurable Cl^-/HCO_3^- exchange begins, there is a relative excess of transfer sites on the outside face which partly compensates for the slower movement of chloride-loaded sites across surface II. Therefore the initial rate of anion exchange is higher than in the steady state and the slippage rate constants determine the relaxation. A similar argument may be made for chloride-loaded ghosts with the same result: the initial velocity exceeds and relaxes to that of the steady state. These considerations suggest that the measured v_0 reflects the state of the membrane a few milliseconds after mixing rather than the theoretical state at $t = 0$, which is what equations 35 and 37 describe. Clearly these factors do not change the general form of the functional dependence of v_0 (Fig. 6) but do suggest areas for further investigation.

In conclusion, we found that Cl^-/HCO_3^- exchange in erythrocyte ghosts does not follow a single exponential at 4°C and extended the usual ping-pong model to include slippage in order to explain this phenomenon. We derived the system of equations resulting from the model and obtained the solution, which is a double exponential function. We have demonstrated that the functional dependence predicted by our model of each rate constant fits the data. Other aspects of the model, such as the amplitudes of the double exponential, and temperature dependence of the rate constants are currently under investigation.

This work was supported in part by the Annie Laurie Charitable Trust Pilot Research Grant (IIRG93-026) from the Alzheimer's Association, in part by a grant from the American Medical Association Education and Research Foundation and by a gift from Philomen T. Marvell, MD. The authors thank Michael Toon for critically reading the manuscript.

References

Alper, S.L. 1991. The band 3-related anion exchanger (AE) gene family. *Ann. Rev. Physiol.* **53:**549–564

Baker, G.F., Baker, P. 1996. Temperature dependence of the exchange of monovalent anions in human red blood cells. *Biochim. Biophys. Acta* **1285:**192–202

Calafut, T.M., Dix, J.A. 1995. Chloride-bicarbonate exchange through the human red cell ghost membrane monitored by the fluorescent probe 6-methoxy-N-(3-sulfopropyl)quinolinium. *Anal. Biochem.* **230:**1–7

Chow, E.I., Crandall, E.D., Forster, R.E. 1976. Kinetics of bicarbonate-chloride exchange across the human red blood cell membrane. *J. Gen. Physiol.* **68:**633–652

Cleland, W.W. 1963. The kinetics of enzyme-catalyzed reactions with two or more substrates. *Biochim. Biophys. Acta* **67:**104–137

Dalmark, M. 1972. The effect of temperature, bicarbonate, carbon dioxide, and pH on the chloride transport across the human red cell membrane. *In:* Oxygen Affinity of Hemoglobin and Red Cell Acid Base Status. M. Rørth and P. Astrup, editors. pp. 320–331. Munksgaard, Copenhagen

Dalmark, M. 1976. Effects of halides and bicarbonate on chloride transport in human red blood cells. *J. Gen. Physiol.* **67:**223–234

Falke, J.J., Chan, S.I. 1985. Evidence that anion transport by band 3 proceeds via a ping-pong mechanism involving a single transport site. *J. Biol. Chem.* **260:**9537–9544

Falke, J.J., Kanes, K.J., Chan, S.I. 1985. The kinetic equation for the chloride transport cycle of band 3. *J. Biol. Chem.* **260:**9545–9551

Fröhlich, O. 1984. Relative contributions of the slippage and tunneling mechanisms to anion net efflux from human erythrocytes. *J. Gen. Physiol.* **84:**877–893

Fröhlich, O., Gunn, R.B. 1986. Erythrocyte anion transport: the kinetics of a single-site obligatory exchange system. *Biochim. Biophys. Acta* **864:**169–194

Fröhlich, O., Leibson, C., Gunn, R. B. 1983. Chloride net efflux from intact erythrocytes under slippage conditions. *J. Gen. Physiol.* **81:** 127–152

Funder, J., Wieth, J.O. 1976. Chloride transport in human erythrocytes and ghosts: a quantitative study. *J. Physiol.* **262:**679–698

Garcia, A.M. 1992. Determination of ion permeability by fluorescence quenching. *Methods Enzymol.* **207:**501–510

Gasbjerg, P.K., Brahm, J. 1991. Kinetics of bicarbonate and chloride transport in human red cell membranes. *J. Gen. Physiol.* **97:**321–349

Gasbjerg, P.K., Knauf, P.A., Brahm, J. 1996. Kinetics of bicarbonate transport in human red blood cell membranes at body temperature. *J. Gen. Physiol.* **108:**565–575

Hunter, M.J. 1977. Human erythrocyte anion permeabilities measured under conditions of net charge transfer. *J. Physiol.* **268:**35–49

Illsley, N.P., Verkman, A.S. 1987. Membrane chloride transport measured using a chloride-sensitive fluorescent probe. *Biochemistry* **26:**1215–1219

Jennings, M.L. 1982. Stoichiometry of a half-turnover of band 3, the chloride transport protein of human erythrocytes. *J. Gen. Physiol.* **79:**169–185

Jennings, M.L. 1992. Cellular anion transport. *In:* The Kidney: Physiology and Pathophysiology, Second Edition, D.W. Seldin and G. Giebisch, editors. pp. 113–145. Raven Press, New York

Klocke, R.A. 1976. Rate of bicarbonate-chloride exchange in human red cells at 37°C. *J. App. Physiol.* **40:**707–714

Knauf, P.A. 1979. Erythrocyte anion exchange and the band 3 protein: transport kinetics and molecular structure. *Curr. Top. Membr. Transp.* **12:**249–363

Knauf, P.A., Gasbjerg, P.K., Brahm, J. 1996. The asymmetry of chloride transport at 38°C in human red blood cell membranes. *J. Gen. Physiol.* **108:**577–589

Knauf, P.A., Law, F., Marchant, P.J. 1983. Relationship of net chloride flow across the human erythrocyte membrane to the anion exchange mechanism. *J. Gen. Physiol.* **81:**95–126

Lambert, A., Lowe, A.G. 1980. Chloride-bicarbonate exchange in human red cells measured using a stopped flow apparatus. *J. Physiol.* **306:**431–443

London, R.D., Lipkowitz, M.S., Abramson, R.G. 1987. Cl^-/HCO_3^- antiporter in red cell ghosts: a kinetic assessment with fluorescent probes. *Am. J. Physiol.* **252:**F844–F855

Magid, E., Turbeck, B.O. 1968. The rates of the spontaneous hydration of CO_2 and the reciprocal reaction in neutral aqueous solutions between 0° and 38°. *Biochim. Biophys. Acta* **165:**515–524

Neame, K.D., Richards, T.G. 1972. Elementary Kinetics of Membrane Carrier Transport. John Wiley & Sons. New York

Passow, H. 1986. Molecular aspects of band 3 protein-mediated anion transport across the red blood cell membrane. *Rev. Physiol. Biochem. Pharmacol.* **103:**61–223

Schultz, S.G. 1980. Basic Principles of Membrane Transport. Cambridge University Press. New York

Schwoch, G., Passow, H. 1973. Preparation and properties of human erythrocyte ghosts. *Molec. Cell. Biochem.* **2:**197–218

Segel, I.H. 1975. Enzyme Kinetics. John Wiley & Sons, New York

Steck, T.L., Kant, J.A. 1974. Preparation of impermeant ghosts and inside-out vesicles from human erythrocyte membranes. *Methods Enzymol.* **31:**172–180

Tanner, M.J.A. 1993. Molecular and cellular biology of the erythrocyte anion exchanger (AE1). *Sem. Hemat.* **30:**34–57

Tosteson, D.C. 1959. Halide transport in red blood cells. *Acta Physiol. Scand.* **46:**19–41

Vassuer, M., Frangne, R., Alvarado, F. 1993. Buffer-dependent pH sensitivity of the fluorescent chloride-indicator dye SPQ. *Am. J. Physiol.* **264:**C27–C31

Zhang, Z., Solomon, A.K. 1992. Effect of pCMBS on anion transport in human red cell membranes. *Biochim. Biophys. Acta* **1106:**31–39

Appendix

The solution to Eq. 31 may be obtained as follows. Substituting the constraints of electroneutrality (Eqs. 20 and 21) into Eqs. 1 and 4 respectively, leads to

$$\frac{dP_U^i}{dt} = j_U^{II} = u_{21} P_U^o - u_{12} P_U^i \tag{A1}$$

and

$$\frac{dP_U^o}{dt} = -j_U^{II} = -u_{21} P_U^o + u_{12} P_U^i \tag{A2}$$

Adding A1 and A2 gives

$$\frac{dP_U^i}{dt} + \frac{dP_U^o}{dt} = 0 \tag{A3}$$

which may be integrated to

$$P_U^i(t) - P_U^i(0) + P_U^o(t) - P_U^o(0) = 0. \tag{A4}$$

Using A4 to solve for $P_U^o(t)$, substituting the result into A1, and integrating leads to

$$P_U^i(t) = \frac{[u_{12}P_U^i(0) - u_{21}P_U^o(0)]}{u_{21} + u_{12}} e^{-(u_{21}+u_{12})t} + \overline{P}_U^i \tag{A5}$$

where we have used $\overline{P}_U^i$ to represent the equilibrium value of P_U^i and the

equation $P_U^i(0) + P_U^o(0) = \overline{P}_U^i + \overline{P}_U^o$ which is a special case of A4. At equilibrium we have

$$\overline{P}_U^o = K_U \overline{P}_U^i \tag{A6}$$

and

$$P^T = \overline{P}_U^o + \overline{P}_C^o + \overline{P}_B^o + \overline{P}_U^i + \overline{P}_C^i + \overline{P}_B^i$$

Substituting equations 24–27 and A6 into the above equation leads, after solving for $\overline{P}_U^i$, to

$$\overline{P}_U^i = \frac{P^T}{1 + K_U + C^o\left(\frac{K_U}{K_C^o} + \frac{1}{K_C^i}\right) + B^o\left(\frac{K_U}{K_B^o} + \frac{1}{K_B^i}\right)} \tag{A7}$$

From the principle of microscopic reversibility we derive the following:

$$\frac{c_{21}}{K_C^o} K_U = \frac{c_{12}}{K_C^i} \tag{A8}$$

In order to utilize the assumption of near equilibrium, we introduce the following first order infinitesimals:

$$\chi = C^i(t) - \overline{C}^i$$

$$\omega = P_U^o(t) - \overline{P}_U^o$$

$$\iota = P_U^i(t) - \overline{P}_U^i$$

Note that $\overline{C}^i = C^o$. From A4 we derive

$$\omega = -\iota \tag{A9}$$

and from (A5) it follows that

$$\frac{d\iota}{dt} = -(u_{21} + u_{12})\iota \tag{A10}$$

Rearranging the definitions of the infinitesimals so that they may be introduced into Eq. 31, dropping all terms with a product of two infinitesimals, and using equations A6 and A8 to simplify terms leads to

$$\frac{d\chi}{dt} + \left(\frac{A}{V^i}\frac{c_{12}}{K_C^i}\overline{P}_U^i\right)\chi = \frac{A}{V^i}\frac{c_{12}}{K_C^i} C^o \left(\frac{u_{21} + u_{12}}{c_{12}} - \frac{1}{K_U} - 1\right)\iota \tag{A11}$$

Rearranging A5 to eliminate ι in A11 gives

$$\frac{d\chi}{dt} + \left(\frac{A}{V^i}\frac{c_{12}}{K_C^i}\overline{P}_U^i\right)\chi = \frac{A}{V^i}\frac{c_{12}}{K_C^i} C^o\left(\frac{u_{21} + u_{12}}{c_{12}} - \frac{1}{K_U} - 1\right)\frac{[u_{12}P_U^i(0) - u_{21}P_U^o(0)]}{u_{21} + u_{12}} e^{-(u_{21}+u_{12})t} \tag{A12}$$

A12 is a linear, first order differential equation whose solution, after replacing χ with $C^i(t) - C^o$, is Eq. 38. Eq. 40 is obtained by use of A7.